

# Dynamics and Multiconfiguration Potential Energy Surface for the Singlet $O_2$ Reactions with Radical Cations of Guanine, 9-Methylguanine, 2'-Deoxyguanosine, and Guanosine

Published as part of *The Journal of Physical Chemistry virtual special issue "Cheuk-Yiu Ng Festschrift"*.

Yan Sun, Midas Tsai, May Myat Moe, and Jianbo Liu\*



Cite This: *J. Phys. Chem. A* 2021, 125, 1564–1576



Read Online

ACCESS |



Metrics & More

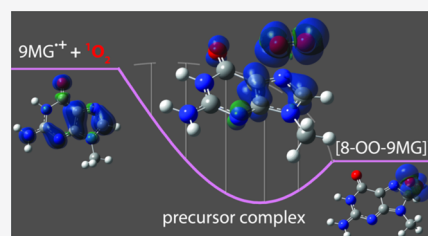


Article Recommendations



Supporting Information

**ABSTRACT:** Reactions of electronically excited singlet oxygen ( $^1O_2$ ) with the radical cations of guanine (9HG $^{\bullet+}$ ), 9-methylguanine (9MG $^{\bullet+}$ ), 2'-deoxyguanosine (dGuo $^{\bullet+}$ ), and guanosine (Guo $^{\bullet+}$ ) were studied in the gas phase by a combination of guided-ion-beam mass spectrometric measurement of product ions and cross sections as a function of collision energy ( $E_{col}$ ) and electronic structure calculations of the reaction potential energy surface (PES) at various levels of theory. No product could be captured in the  $^1O_2$  reaction with bare 9HG $^{\bullet+}$  or 9MG $^{\bullet+}$ , because energized products decayed rapidly to reactants before being detected. To overcome this unfavorable kinetics, monohydrated 9HG $^{\bullet+} \cdot H_2O$  and 9MG $^{\bullet+} \cdot H_2O$  were used as reactant ions, of which the peroxide product ions were stabilized by energy relaxation *via* elimination of the water ligand. Reaction cross sections for 9HG $^{\bullet+} \cdot H_2O$  and 9MG $^{\bullet+} \cdot H_2O$  decrease with increasing  $E_{col}$ , becoming negligible above 0.6 eV. This indicates that the reactions are exothermic with no barriers above reactants and the heat of formation of the products is sufficiently large to overcome their water ligand elimination energy (0.7 eV). Peroxide product ions were also detected in the  $^1O_2$  reactions with unhydrated dGuo $^{\bullet+}$  and Guo $^{\bullet+}$ , in which intramolecular vibrational redistribution was able to stabilize oxidation products. 9MG $^{\bullet+}$  was utilized as a model system to explore the reaction PES for the initial  $^1O_2$  addition to the guanine radical cation. Calculations were carried out using single-reference  $\omega$ B97XD, RI-MP2, and DLPNO-CCSD(T) and multireference CASSCF and CASPT2. Although the same PES profile was obtained at different levels of theory, the energies of the mixed open- and closed-shell  $^1O_2$  reactant and the open-shell reaction intermediates, transition states, and products are sensitive to the theories. By taking into account both static and dynamic electron correlations, the CASPT2 PES has provided the best agreement with the experimentally measured reaction thermodynamics and predicted 8-peroxide as the most probable initial oxidation product of the guanine radical cation.



## 1. INTRODUCTION

Compared to the adenine (A), cytosine (C), and thymine (T) nucleobases, guanine (G) has the lowest oxidation potential ( $E^\circ$  vs NHE = 1.29 V for guanosine, 1.42 V for adenosine, 1.6 V for deoxycytidine, and 1.7 V for thymidine)<sup>1,2</sup> and the lowest adiabatic ionization energy (AIE = 7.75 eV for G, 8.27 eV for A, 8.66 eV for C, and 8.82 eV for T).<sup>3,4</sup> This makes guanine the primary target for one-electron oxidation, leading to the facile formation of guanine radical cation ( $G^{\bullet+}$ ) upon radiolysis,<sup>5,6</sup> photolysis,<sup>7</sup> chemical oxidation,<sup>8</sup> electron transfer between DNA-bound metal complexes,<sup>9</sup> electrocatalytic oxidation,<sup>10,11</sup> and type I photosensitized oxidation.<sup>12,13</sup> The complementary base pairing of G with C in double-helical DNA further reduces its  $E^\circ$  by 0.28–0.34 V<sup>14,15</sup> and AIE by 0.75–0.78 eV.<sup>16,17</sup> In line with these facts, electron holes that are initially created by one-electron oxidation of other nucleobases may migrate for long distances from the locus of formation to the guanine sites,<sup>18</sup> rendering the formation of  $G^{\bullet+}$  as an ultimate trap for the oxidative damage to DNA.<sup>6</sup> Formation of  $G^{\bullet+}$  is the first step toward a variety of biological

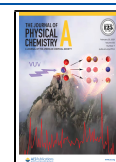
sequelae,<sup>19–22</sup> most of which are highly mutagenic, *e.g.*, 8-oxo-7,8-dihydroguanine (8-OG, the most common product produced *in vivo* under oxidative stress<sup>23</sup>) lesion<sup>20</sup> in genomic, mitochondrial, and telomeric DNA.

Of relevance to the guanine-mediated DNA lesions is the electronically excited singlet oxygen ( $O_2[a^1\Delta_g]$ )-induced damage.  $^1O_2$  is generated in living systems through enzymatic and nonenzymatic reactions, type II photosensitization, chemical excitation, *etc.*<sup>24,25</sup> and is known to cause DNA damage.<sup>20,26–29</sup> The  $^1O_2$  damage to DNA initiates exclusively at the guanine residues.<sup>20–22,26–48</sup> The consequential primary and secondary damage is implicated in DNA strand breaks,<sup>2</sup> DNA–protein cross-links,<sup>43,48</sup> mutation,<sup>49</sup> and apoptosis<sup>50</sup> as

Received: January 5, 2021

Revised: February 3, 2021

Published: February 11, 2021



well as in photodynamic therapy for cancer.<sup>51</sup> Most of the mechanistic insights on the  $^1\text{O}_2$  oxidation of guanine were obtained from the measurements of guanine residues in various contexts (including isolated nucleobases, nucleosides, oligonucleotides, and single- and double-stranded DNA) in solution<sup>26–40,47,48</sup> and their protonated and deprotonated ions in the gas phase,<sup>44–46</sup> augmented by reaction potential energy surface (PES) investigations<sup>43–48,52,53</sup> and molecular dynamics simulations.<sup>41,42,44–46</sup> A currently accepted mechanism is that guanine is attacked by  $^1\text{O}_2$  on its imidazole ring, forming a transient peroxide and/or endoperoxide that quickly converts to a hydroperoxide 8-OOH-G. The 8-OOH-G in isolated nucleosides and short oligonucleotides undergoes a series of reactions and ultimately forms spiroiminodihydantoin and guanidinohydantoin;<sup>35</sup> whereas that within DNA is reduced to 8-OG.<sup>28</sup> A scenario of biological significance is ionizing radiation and/or one-electron oxidants interacting with DNA in the presence of  $^1\text{O}_2$ . Under that circumstance, synergistic effects from the combination of  $\text{G}^{\bullet+}$  formation and  $^1\text{O}_2$  oxidation are anticipated. Surprisingly, the reaction of  $\text{G}^{\bullet+}$  with  $^1\text{O}_2$  has not yet been directly measured or theoretically modeled. Neither the reaction kinetics nor the nature of the oxidation products was known. On the other hand, the knowledge of such concurrent processes is not only of significance for the fundamental understanding of DNA oxidatively generated damage but also of high practical interest in exploring the additive effects of combining ionization radiation-based radiotherapy and  $^1\text{O}_2$ -based photodynamic therapy in cancer treatment.<sup>54–56</sup>

The degradation pathways of  $\text{G}^{\bullet+}$  depend on structural context and reaction environments (*i.e.*, solvent and pH). In neutral aqueous solution, free  $\text{G}^{\bullet+}$  (and that within single-stranded DNA) undergoes deprotonation through the loss of the imino proton at N1 to water and yields a neutral radical  $[\text{G} - \text{H}]^\bullet$  within 56 ns.<sup>57,58</sup> In contrast,  $\text{G}^{\bullet+}$  within double-stranded DNA is stabilized through Watson–Crick base pairing which diminishes the probability of deprotonation.<sup>59</sup> The fates of  $\text{G}^{\bullet+}$  and  $[\text{G} - \text{H}]^\bullet$  are distinctively different by following different transformations and producing different end products.<sup>19–22</sup> This implies that a direct measurement of  $\text{G}^{\bullet+}$  with  $^1\text{O}_2$  in aqueous solution is not feasible, because deprotonation of  $\text{G}^{\bullet+}$  may be faster than oxidation and the oxidation behavior of deprotonated  $[\text{G} - \text{H}]^\bullet$  may not faithfully mimic that of  $\text{G}^{\bullet+}$  within DNA.<sup>6</sup> In this sense, a gas-phase environment is more appropriate for examining the  $^1\text{O}_2$  oxidation of  $\text{G}^{\bullet+}$  wherein deprotonation shuts down and reaction is not perturbed by solvent and counterions. In the present work, the reactions of  $^1\text{O}_2$  with the radical cations of guanine (9HG $^{\bullet+}$ ), 9-methylguanine (9MG $^{\bullet+}$ ), 2'-deoxyguanosine (dGuo $^{\bullet+}$ ), and guanosine (Guo $^{\bullet+}$ ) were investigated in the gas phase, in the order of increasing structural complexity. The guided-ion-beam scattering mass spectrometric measurement, combined with multiconfiguration reaction PES modeling, constituted the first study on the chemistry of the guanine radical cation with  $^1\text{O}_2$ .

## 2. EXPERIMENTAL AND THEORETICAL METHODS

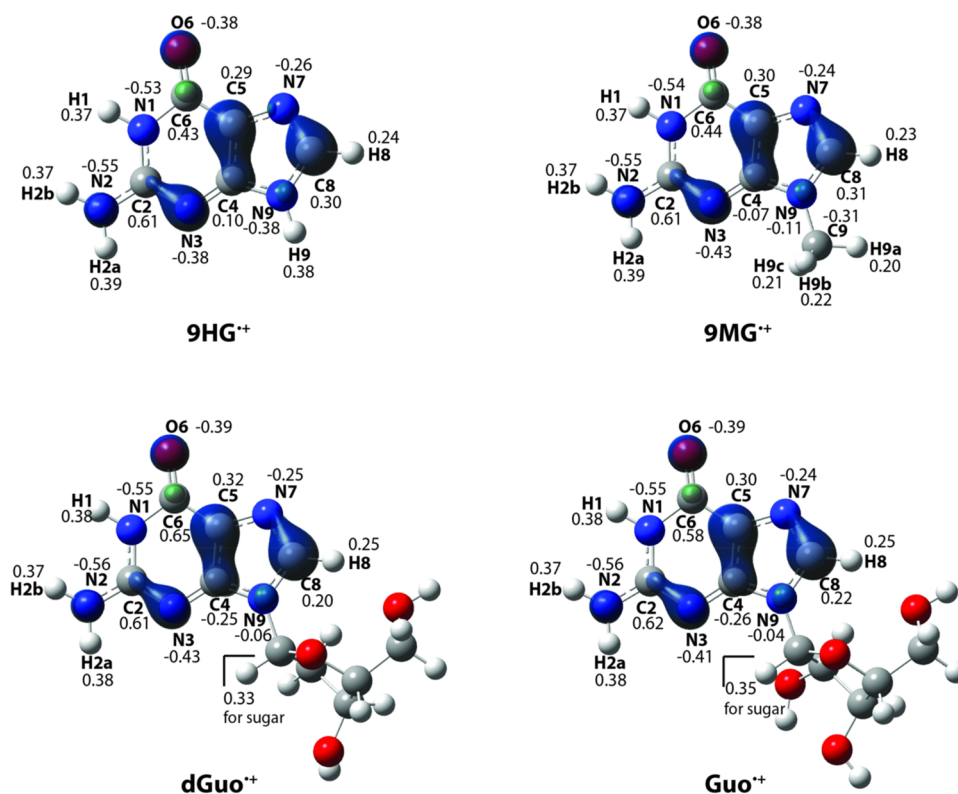
**2.1. Chemicals.** 9MG (Aldrich, > 98.0%), dGuo (Sigma, > 99%), Guo (Acros, 99%),  $\text{Cu}(\text{NO}_3)_2$  (Alfa Aesar, 99.999%), KOH (Fisher Chemical, > 85%), and aqueous  $\text{H}_2\text{O}_2$  (Acros Organics, 35 wt %) were used without further purification. Chlorine gas (99.5%) was purchased from Sigma-Aldrich, and

helium gas (research grade) was purchased from T.W. Smith. All solvents were HPLC grade.

**2.2. Generation and Detection of  $^1\text{O}_2$ .**  $^1\text{O}_2$  was generated by the reaction of  $\text{H}_2\text{O}_2 + \text{Cl}_2 + 2\text{KOH} \rightarrow ^1\text{O}_2/^3\text{O}_2 + 2\text{KCl} + 2\text{H}_2\text{O}$ .<sup>60,61</sup> In brief, 10.5 mL of 8 M KOH was added to 20 mL of 35 wt % aqueous  $\text{H}_2\text{O}_2$  in a sparger held at  $-18\text{ }^\circ\text{C}$ . The mixture was degassed, and 3.42 sccm of  $\text{Cl}_2$  was mixed with 53.5 sccm of He in a gas proportioner and bubbled through the  $\text{H}_2\text{O}_2/\text{KOH}$  slush.  $\text{Cl}_2$  reacted completely with  $\text{H}_2\text{O}_2$  and produced a mixture of  $^1\text{O}_2$ ,  $^3\text{O}_2$ , and water. Gas products passed through a cold trap (kept at  $-70\text{ }^\circ\text{C}$ ) to remove water vapor. Only  $^1\text{O}_2$ ,  $^3\text{O}_2$ , and He remained in the downstream gas. The concentration of  $^1\text{O}_2$  was determined by measuring its  $a^1\Delta_g \rightarrow X^3\Sigma_g^-$  emission<sup>62</sup> in an optical emission cell. Emission from the cell was collimated, passed through an optical chopper, and filtered by a 5 nm bandwidth interference filter centered at 1270 nm. The chopped emission was focused into a thermoelectrically cooled InGaAs photodetector (Newport 71887 detector and 77055 cooler) coupled with a lock-in amplifier (SRS model SR830). The amplifier output was converted to absolute  $^1\text{O}_2$  concentration per a previous calibration.<sup>63</sup> To reduce wall- and self-quenching of  $^1\text{O}_2$ , the sparger was continuously evacuated and its pressure was maintained at 12.8  $\tau$ . At this pressure, a steady concentration of  $^1\text{O}_2$  (up to 15%) was produced for conducting ion–molecule reactions.

**2.3. Formation of Guanine Radical Cation and Ion–Molecule Scattering.** Reaction of guanine radical cation with  $^1\text{O}_2$  was carried out on a homemade electrospray ionization (ESI) guided-ion-beam scattering tandem mass spectrometer at Queens College. Details of the apparatus can be found in our previous work.<sup>64,65</sup> As a source of guanine radical cations, we used collision-induced-dissociation (CID) of  $\text{Cu}(\text{II})$ -nucleoside complexes.<sup>65–67</sup> A methanol/water (*v:v* = 3:1) solution of 0.25 mM  $\text{Cu}(\text{NO}_3)_2$  and 0.5 mM guanosine was freshly prepared and sprayed into the air through an ESI needle at a rate of 0.06 mL/h. The  $[\text{Cu}^{\text{II}}(\text{Guo})_{0-6}]^{\bullet+}$  ( $\text{CH}_3\text{OH}$ )<sub>0-3</sub> complexes formed in the electrospray entered the source chamber of the mass spectrometer through a desolvation capillary which was biased at 115 V with respect to ground and heated to 200  $^\circ\text{C}$ . The source chamber was evacuated to a pressure of 1.7  $\tau$ . A 1.0 mm orifice skimmer was located 3 mm from the end of the desolvation capillary, separating the source chamber and a hexapole ion guide. The skimmer was biased at 17 V with respect to ground. The electrical field between the capillary and the skimmer prompted CID of  $[\text{Cu}^{\text{II}}(\text{Guo})_{0-6}]^{\bullet+} \cdot (\text{CH}_3\text{OH})_{0-3}$  with the background gas in the source chamber, and the dissociation of  $[\text{Cu}^{\text{II}}(\text{Guo})_3]^{\bullet+}$  was featured by redox separation, *i.e.*,  $[\text{Cu}^{\text{II}}(\text{Guo})_3]^{\bullet+} \rightarrow [\text{Cu}(\text{Guo})_2]^+ + \text{Guo}^{\bullet+}$ . A fraction of  $\text{Guo}^{\bullet+}$  ions eliminated the sugar group ( $-\text{C}_5\text{H}_8\text{O}_4$ ) in CID and produced 9HG $^{\bullet+}$ . Likewise, 9MG $^{\bullet+}$  and dGuo $^{\bullet+}$  were generated by CID of  $[\text{Cu}^{\text{II}}(9\text{MG})_3]^{\bullet+}$  and  $[\text{Cu}^{\text{II}}(\text{dGuo})_3]^{\bullet+}$ , for which the ESI solution was prepared using 9MG and dGuo, respectively.

Radical cations were transported into the hexapole ion guide for collisional focusing and thermalization to 310 K, followed by mass selection in a quadrupole mass filter. Mass-selected reactant radical ions were injected into an octopole ion guide that passes a scattering cell containing the  $^1\text{O}_2$  reactant. In addition to providing radio frequency potential that traps ions in the radial direction, the octopole was biased at a variable DC

Scheme 1. Lowest-Energy Structures of 9HG<sup>•+</sup>, 9MG<sup>•+</sup>, dGuo<sup>•+</sup>, and Guo<sup>•+</sup> Optimized at the  $\omega$ B97XD/6-31+G(d,p) Level of Theory, with Atomic Numbering Schemes<sup>a</sup>

<sup>a</sup>Spin densities are represented by contour plots, and charge densities are indicated by the numbers. Their Cartesian coordinates are available in the Supporting Information.

potential. The DC offset controlled the kinetic energy of reactant ions in the laboratory frame ( $E_{\text{lab}}$ ) and thereby set the collision energy ( $E_{\text{col}}$ ) between radical cations and  $^1\text{O}_2$  in the center-of-mass frame using  $E_{\text{col}} = E_{\text{lab}} \times m_{\text{neutral}} / (m_{\text{ion}} + m_{\text{neutral}})$ , where  $m_{\text{ion}}$  and  $m_{\text{neutral}}$  stand for the masses of ionic and neutral reactants, respectively. After ion–molecule scattering, the product ions resulting from the reaction and the remaining reactant ions were collected by the octopole, passed into a second quadrupole mass filter for mass analysis, and counted by an electron multiplier detector. Reaction cross sections were calculated from the ratio of reactant/product ion intensities at each  $E_{\text{col}}$ , the pressure and the concentration of  $^1\text{O}_2$  in the scattering cell, and the effective cell length. The scattering cell gas pressure (including  $^1\text{O}_2$ ,  $^3\text{O}_2$ , and He) was maintained at 0.25 mT. At this pressure, guanine radical cations had at most single collisions with oxygen molecules. It was reported that the guanine radical cation does not present observable reaction with  $^3\text{O}_2$ .<sup>68</sup> The nonreactivity for the collisions of 9HG<sup>•+</sup>, 9MG<sup>•+</sup>, dGuo<sup>•+</sup>, and Guo<sup>•+</sup> with  $^3\text{O}_2$  was further verified in our control experiment conducted under the same conditions except that  $^1\text{O}_2$  was replaced by  $^3\text{O}_2$  gas.

The ion beam intensities were  $3 \times 10^5$  cps for 9HG<sup>•+</sup>,  $8 \times 10^5$  cps for 9MG<sup>•+</sup>, and  $3 \times 10^5$  cps for dGuo<sup>•+</sup> and Guo<sup>•+</sup>. Initial kinetic energy of the ion beam was set at 0.8 eV, with an energy spread controlled to be <0.7 eV by collisional damping in the hexapole and reducing the radius of the ion beam at the exit of the first quadrupole. Monohydrated 9HG<sup>•+</sup>·H<sub>2</sub>O and 9MG<sup>•+</sup>·H<sub>2</sub>O were generated in a similar procedure, except that the sample solution was prepared in 2:1 methanol/water. The

ion intensities were  $2.4 \times 10^4$  and  $4 \times 10^4$  cps for 9HG<sup>•+</sup>·H<sub>2</sub>O and 9MG<sup>•+</sup>·H<sub>2</sub>O, respectively.

**2.4. Electronic Structure Calculations.** 9MG<sup>•+</sup> was utilized as a prototype for modeling guanosine radical cation reaction PES, of which the N9-methyl group mimics the nucleoside sugar moiety. As demonstrated in Scheme 1, 9MG<sup>•+</sup> has the same nucleobase conformation and the same spin density distribution (*i.e.*, an unpaired electron is delocalized among N3, C4, C5, and C8) as those of dGuo<sup>•+</sup> and Guo<sup>•+</sup>.<sup>65</sup> It is thus reasonable to assume that the methyl-substitution at N9 has little effect on the relative enthalpies of oxidation intermediates, transition states (TSs), and products of guanosine,<sup>52</sup> as verified in our experiment. Geometries of reactants, intermediates, TSs, and products were optimized using the  $\omega$ B97XD<sup>69</sup> density functional theory (DFT) paired with the 6-31+G(d,p) basis set. This range-separated functional mitigates self-interaction errors and improves the orbital description of radical ions<sup>70</sup> in comparison to the B3LYP functional. The latter is known to introduce severe spin contamination in the 9MG<sup>•+</sup> reactant.<sup>71</sup>

The challenge in the calculation of PES for the guanine radical cation with  $^1\text{O}_2$  is that the system presents multi-configuration wave functions originating from the mixed open- and closed-shell character of  $^1\text{O}_2$ .<sup>72</sup> The spin-restricted DFT is unable to describe the static correlation arising from the two degenerate  $\pi^*$  antibonding orbitals and overestimates the  $^1\text{O}_2$  excitation energy, whereas the broken-symmetry, spin-unrestricted DFT brings about spin contamination from the ground-state  $^3\text{O}_2$ . This problem exists not only in the  $^1\text{O}_2$  reactant but also in the intermediates and TSs for  $^1\text{O}_2$  addition



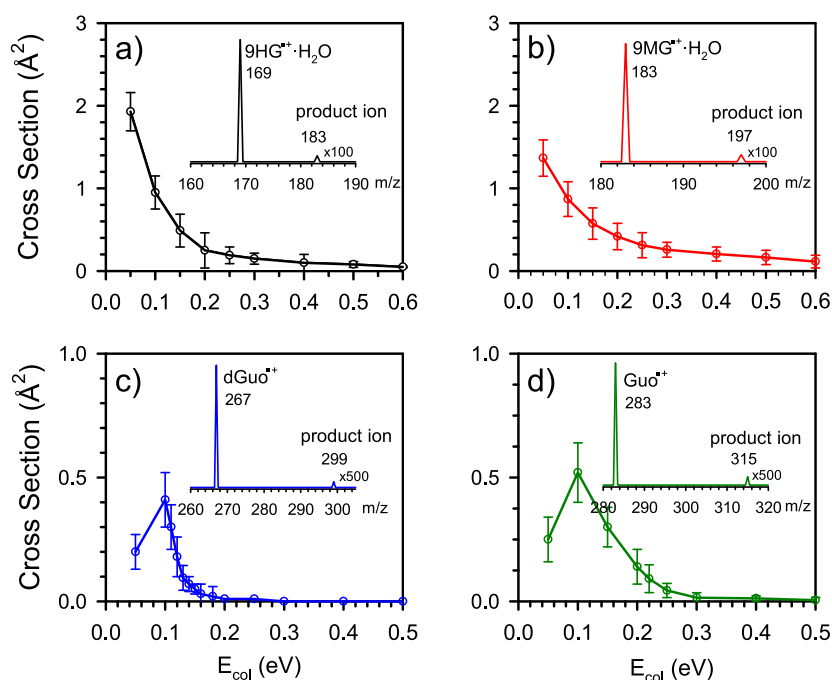


**Figure 1.** Product cross sections for the <sup>1</sup>O<sub>2</sub> reactions with (a) 9HG<sup>•+</sup>·H<sub>2</sub>O, (b) 9MG<sup>•+</sup>·H<sub>2</sub>O, (c) dGuo<sup>•+</sup>, and (d) Guo<sup>•+</sup>. Insets show product ion mass spectra.

to guanine.<sup>43,46–48</sup> In our previous study of the <sup>1</sup>O<sub>2</sub> reactions with protonated and deprotonated guanine ions,<sup>46–48</sup> spin contamination in the PES was corrected using Yamaguchi's approximate spin-projection method,<sup>73,74</sup> in which the spin-projected total electronic energy of an open-shell singlet state was calculated as a weighted combination of broken-symmetry, spin-unrestricted singlet and triplet states. However, the approximate spin-projection was validated only for systems containing singlet and triplet states.<sup>43,46,47,73,74</sup> The present system, on the other hand, is more complicated in that it mixes doublet and quartet states.

To obtain a reliable PES and therefore identify minimum energy reaction pathway(s), we have adopted a composite and more rigorous procedure in this work. DFT calculations at the  $\omega$ B97XD/6-31+G(d,p) level were employed to map out all possible reaction pathways for the <sup>1</sup>O<sub>2</sub>-addition to 9MG<sup>•+</sup> and optimize all stationary points along reaction coordinates. All TSs were verified as first-order saddle points, and the vibrational mode associated with an imaginary frequency corresponds to the anticipated reaction pathway. Intrinsic reaction coordinate (IRC) calculation was carried out to substantiate reactant/product minima connected through each TS. Once reaction pathways were identified, electronic energies of all stationary structures and TSs were refined. First, two high-level, single-reference methods were applied for single-point energy calculations: the resolution-of-the-identity second-order Møller–Plesset perturbation theory (RI-MP2/aug-cc-pVQZ)<sup>75,76</sup> and the domain-based local pair-natural orbital coupled-cluster single-, double- and perturbative triple-excitation method (DLPNO-CCSD(T)/aug-cc-pVTZ, where the inclusion of a perturbative correction for triple excitation may compensate for the deficiencies of a single-determinant reference).<sup>77</sup> Energies were further examined using the multireference complete active space self-consistent field method,<sup>78,79</sup> *i.e.*, CASSCF(9,7)/6-31+G(d,p) for 9MG<sup>•+</sup>, CASSCF(12,8)/6-31+G(d,p) for <sup>1</sup>O<sub>2</sub>, and CASSCF(21,15)/

6-31+G(d,p) for other reaction species where the  $\sigma_{O(2s)-O(2s)}$ ,  $\sigma_{O(2s)-O(2s)}^*$ ,  $\sigma_{O(2p)-O(2p)}$ ,  $\pi_{\pm 1}$ ,  $\pi_{\pm 1}^*$ , and  $\sigma_{O(2p)-O(2p)}^*$  orbitals of O<sub>2</sub> and the  $\pi$  orbitals of the guanine imidazole ring were included in the active space. Reaction enthalpy ( $\Delta H$ ) reported at each level of theory is based on the sum of the electronic energy calculated at the specified level and the 298 K thermal correction at  $\omega$ B97XD/6-31+G(d,p) (including zero-point energy which was scaled by a factor of 0.975<sup>80</sup>).

As we had expected, although all single- and multireference methods predicted similar reaction coordinates, reaction potential energies were very sensitive to the theories. Particularly, the CASSCF calculations located most reaction intermediates and TSs above the reactants in energy, which was inconsistent with our experimental finding that the reaction is exothermic. The issue with the CASSCF calculations is that the electron correlation energy was treated in an unbalanced way, and only that corresponding to the active orbitals (*i.e.*, static correlation) was considered. To take into account both static and dynamic correlations, we have proceeded to calculate the reaction PES using CASPT2-(21,15)/6-31G(d,p),<sup>81,82</sup> *i.e.*, adding remaining dynamic correlation using second-order perturbation theory with the CASSCF wave function as the reference. Because CASPT2 treats dynamic correlation effects perturbatively, it is less expensive than the multireference configuration interaction (MRCI) method<sup>83</sup> and allows for handling a large number of active orbitals for correlation.<sup>81,82</sup>

The  $\omega$ B97XD/6-31+G(d,p) and CASSCF(21,15)/6-31+G(d,p) calculations were completed using Gaussian 09.<sup>84</sup> Electronic energies at the RI-MP2/aug-cc-pVQZ and DLPNO-CCSD(T)/aug-cc-pVTZ levels of theory were calculated with ORCA 4.<sup>85</sup> The CASPT2(21,15)/6-31G(d,p) calculations were carried out using MOLCAS 8,<sup>86</sup> for which the shift parameter for ionization potential–electron affinity (IPEA) was set to 0.25 au.<sup>87,88</sup>

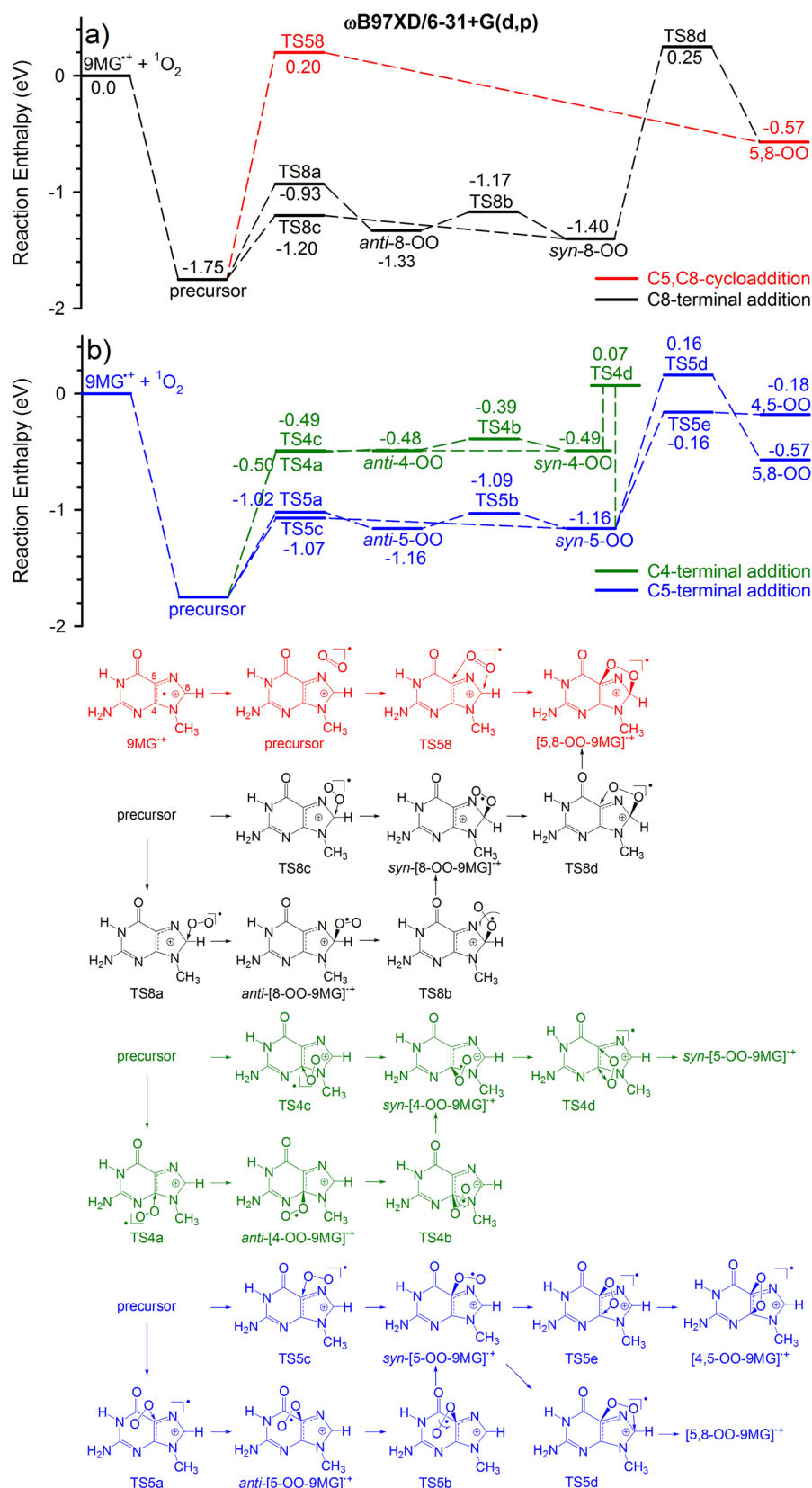


**Figure 2.** Reaction pathways for the  $^1\text{O}_2$  addition to  $9\text{MG}^{\bullet+}$ . Structures and reaction enthalpies were calculated at the  $\omega$ B97XD/6-31+G(d,p) level of theory, including thermal corrections at 298 K. For TSs, the vibrational mode corresponding to the imaginary frequency is indicated by displacement vectors in the ChemDraw structures. Cartesian coordinates for the calculated structures are available in the Supporting Information.

### 3. RESULTS AND DISCUSSION

**3.1. Reaction Products and Cross Sections.** **3.1.1.  $^1\text{O}_2$  with  $9\text{HG}^{\bullet+}$  and  $9\text{MG}^{\bullet+}$ .** We first measured the ion–molecule scattering of  $9\text{HG}^{\bullet+}$  and  $9\text{MG}^{\bullet+}$  with  $^1\text{O}_2$ . For both systems, no products were detected over an  $E_{\text{col}}$  range from 0.05 to 1.0 eV except collision-induced fragment ions of the ionic reactants. A similar scenario was observed previously that no oxidation products were detected for the  $^1\text{O}_2$  reactions with  $[9\text{HG} + \text{H}]^+$ ,  $[9\text{MG} + \text{H}]^+$ ,  $[9\text{HG} - \text{H}]^-$ , and  $[9\text{MG} - \text{H}]^-$  ions.<sup>44,45</sup> The rationalization is that the nascent endoperoxide and/or exoperoxide adducts of guanine ions were energized by the reaction exothermicity and completely decayed back to the starting reactants during their time-of-flight within the mass spectrometer ( $\sim 500 \mu\text{s}$ ). In order to overcome this unfavorable reaction kinetics, we have employed an alternative method by using monohydrated reactant ions as the target for collisions with  $^1\text{O}_2$ . The idea was to enhance the energy relaxation of oxidation intermediates, *i.e.*, the reaction heat of formation, which would otherwise prompt the decomposition of an  $\text{O}_2$ -adduct, was used up mostly for eliminating a water ligand and the accompanying product kinetic energy release. By employing the water-evaporation cooling strategy, we have indeed observed the reaction products of  $^1\text{O}_2$  with  $9\text{HG}^{\bullet+}\cdot\text{H}_2\text{O}$  and  $9\text{MG}^{\bullet+}\cdot\text{H}_2\text{O}$ . Product ions were detected at  $m/z = 183$  for  $9\text{HG}^{\bullet+}\cdot\text{H}_2\text{O} + ^1\text{O}_2$  and  $m/z = 197$  for  $9\text{MG}^{\bullet+}\cdot\text{H}_2\text{O} + ^1\text{O}_2$ , each of which corresponds to the liberation of a water ligand from an  $\text{O}_2$ -adduct of the hydrated reactant ion.

Figure 1a,b shows the product ion cross sections for  $9\text{HG}^{\bullet+}\cdot\text{H}_2\text{O} + ^1\text{O}_2$  and  $9\text{MG}^{\bullet+}\cdot\text{H}_2\text{O} + ^1\text{O}_2$  as a function of  $E_{\text{col}}$  from 0.05 to 0.6 eV. Error bars were estimated on the basis of 4 sets of measurements. Insets present representative product ion mass spectra measured at  $E_{\text{col}} = 0.05$  eV, where the product ion peaks were scaled by a factor of 100 for clarity. For both reaction systems, the product ion cross section decreases with increasing  $E_{\text{col}}$ , indicating that these reactions are exothermic and there are no activation barriers above the reactants. The fact that the reactions are able to eliminate a water ligand from the product complexes also indicates that the exothermicities of the oxidation reactions are more than the water binding energies of the products (0.7 eV, see below). This thermodynamic data will serve as experimental evidence to benchmark PES computation.

Reaction efficiency, estimated by  $\sigma_{\text{reaction}}/\sigma_{\text{collision}}$  (where  $\sigma_{\text{collision}}$  represents the ion-induced dipole capture cross section<sup>89</sup>), is 2% for  $9\text{HG}^{\bullet+}\cdot\text{H}_2\text{O}$  and 1.4% for  $9\text{MG}^{\bullet+}\cdot\text{H}_2\text{O}$  at  $E_{\text{col}} = 0.05$  eV, decreasing to 1.4% for  $9\text{HG}^{\bullet+}\cdot\text{H}_2\text{O}$  and 1.3% for  $9\text{MG}^{\bullet+}\cdot\text{H}_2\text{O}$  at 0.1 eV. Both reactions have become negligible above 0.6 eV. It appears that the 9-methyl substitution inhibits guanine oxidation.

**3.1.2.  $^1\text{O}_2$  with  $\text{dGuo}^{\bullet+}$  and  $\text{Guo}^{\bullet+}$ .** We then measured the scattering of  $\text{dGuo}^{\bullet+}$  and  $\text{Guo}^{\bullet+}$  by  $^1\text{O}_2$ . In contrast to  $9\text{HG}^{\bullet+}$  and  $9\text{MG}^{\bullet+}$ , the  $\text{O}_2$ -addition product ions were captured for both  $\text{dGuo}^{\bullet+}$  and  $\text{Guo}^{\bullet+}$  in their unhydrated states. This is probably due to the larger molecular size of  $\text{dGuo}^{\bullet+}$  and  $\text{Guo}^{\bullet+}$  than  $9\text{HG}^{\bullet+}$  and  $9\text{MG}^{\bullet+}$  and consequently the more efficient intramolecular vibration redistribution (IVR) which helped deposit reaction heat of formation over vibrational modes without decomposing the products.

Figure 1c,d presents product ion mass spectra and cross sections for  $\text{dGuo}^{\bullet+}$  and  $\text{Guo}^{\bullet+}$  over the  $E_{\text{col}}$  range of 0.05–0.5 eV. For both systems, the cross section generally increases with decreasing collision energy, but it dips at the lowest  $E_{\text{col}}$ . The

dip is most likely artificial. To achieve an  $E_{\text{col}}$  below 0.1 eV in the center-of-mass frame, a retarding DC potential was applied to the octopole ion guide to decelerate the reactant ions. Because of the kinetic energy spread ( $\sim 0.7$  eV) of the ion beam, at the lowest  $E_{\text{col}}$  some reactant ions had nearly zero or backward axial velocity in the laboratory frame. This decreased the ion collection efficiency and consequently affected cross-sectional measurement at the lowest  $E_{\text{col}}$ . The problem turned out to be more severe for  $\text{dGuo}^{\bullet+}$  and  $\text{Guo}^{\bullet+}$  than for  $9\text{HG}^{\bullet+}$  and  $9\text{MG}^{\bullet+}$ .

Overall, the  $E_{\text{col}}$  dependence of product cross sections indicates that the  $^1\text{O}_2$  reactions with  $\text{dGuo}^{\bullet+}$  and  $\text{Guo}^{\bullet+}$  are exothermic, analogous to those with  $9\text{HG}^{\bullet+}$  and  $9\text{MG}^{\bullet+}$ . Taking into account the experimental uncertainties, the product cross sections for  $\text{dGuo}^{\bullet+}$  and  $\text{Guo}^{\bullet+}$  are comparable to each other. But they are approximately only half of those for  $9\text{HG}^{\bullet+}\cdot\text{H}_2\text{O}$  and  $9\text{MG}^{\bullet+}\cdot\text{H}_2\text{O}$ . It is possible that, without additional energy relaxation such as water-evaporation cooling in a hydrated system, a fraction of nucleoside product ions have decomposed to the reactants before reaching the mass spectrometer detector. We have attempted to measure the  $^1\text{O}_2$  reactions with  $\text{dGuo}^{\bullet+}\cdot\text{H}_2\text{O}$  and  $\text{Guo}^{\bullet+}\cdot\text{H}_2\text{O}$ , but the beam intensities of monohydrated nucleoside radical cations were too low ( $<10^4$  cps) to allow for meaningful measurements.

**3.2. PES for the  $^1\text{O}_2$  Addition to  $9\text{MG}^{\bullet+}$ .** **3.2.1. Overview of Reaction Pathways and Products.** PES for  $9\text{MG}^{\bullet+}$  with  $^1\text{O}_2$  was explored first using the  $\omega\text{B97XD}/6\text{-}31\text{+G}(\text{d,p})$  method. The one-dimensional PES of the resulting pathways is depicted in Figure 2, including ChemDraw structures of all reaction intermediates, TSs, and products. Cartesian coordinates for these species are provided in the Supporting Information. Four  $^1\text{O}_2$ -addition mechanisms were identified, and all of them are initiated at a reactant-like,  $\pi$ -stacked precursor complex:

(1) Concerted Diels–Alder cycloaddition of  $\text{O}_2$  across the imidazole C5–C8 bond. The reaction is mediated by TS58 and leads to the formation of a 5,8-endoperoxide ( $[\text{5,8-OO-9MG}]^{\bullet+}$ ), as illustrated by the red line in Figure 2a. Along the reaction coordinate, the unpaired electron diffuses from the guanine moiety to the  $\text{O}_2$  orbital as verified by the DFT-calculated spin density distribution and the CASSCF-calculated singly occupied molecular orbital (SOMO), but the positive charge remains at the guanine imidazole ring. Therefore, spin and charge are separating in the reaction. To emphasize that the spin density is delocalized throughout the system, the superscript “ $\bullet+$ ” is applied over the whole reaction structure that is bracketed together. We have explored the possibility of forming a 4,8-endoperoxide, as the latter structure is known to form in the  $^1\text{O}_2$  cycloaddition to neutral guanine and guanosine.<sup>30,43</sup> However, a  $[\text{4,8-OO-9MG}]^{\bullet+}$ -like geometry converged to either  $[\text{5,8-OO-9MG}]^{\bullet+}$  or  $[\text{8-OO-9MG}]^{\bullet+}$ .

(2) C8-terminal addition of  $\text{O}_2$  (shown by black lines in Figure 2a). There are two possible routes which lead to the same product structure but with the *anti*- and *syn*-configurations, respectively, with respect to the imidazole ring.  $^1\text{O}_2$  may attack at the C8 terminal *via* TS8a to produce *anti*- $[\text{8-OO-9MG}]^{\bullet+}$ , followed by interconversion to *syn*- $[\text{8-OO-9MG}]^{\bullet+}$  *via* a rotation barrier TS8b. Alternatively, *syn*- $[\text{8-OO-9MG}]^{\bullet+}$  may be formed directly from the reactants by crossing over TS8c. Compared to that of *anti*- $[\text{8-OO-9MG}]^{\bullet+}$ , the formation of *syn*- $[\text{8-OO-9MG}]^{\bullet+}$  has a lower activation barrier and higher exothermicity and thus is more kinetically

**Table 1. Relative Enthalpies (eV, 298 K) of Reaction Species Calculated at the Single- and Multi-Reference Levels of Theory and Their T1 Diagnostic**

species	$\omega$ B97XD/ 6-31+G(d,p)	RI-MP2/ aug-cc-pVQZ <sup>a</sup>	DLPNO-CCSD(T)/ aug-cc-pVTZ <sup>a</sup>	CASSCF(21,15)/ 6-31+G(d,p) <sup>a,b</sup>	CASPT2(21,15) 6-31G(d,p) <sup>a,c</sup>	T1 diagnostic
9MG <sup>•+</sup> + <sup>1</sup> O <sub>2</sub>	0.0	0.0	0.0	0.0	0.0	0.019 (9MG <sup>•+</sup> ) 0.015 ( <sup>1</sup> O <sub>2</sub> )
precursor	-1.75	-1.38	-0.64	-0.95	-1.16	0.027
TSS8	0.20	-0.26	0.35	1.61	0.71	0.018
[5,8-OO-9MG] <sup>•+</sup>	-0.57	-0.72	-0.48	0.45	0.21	0.016
TS8a	-0.93	0.20	-0.66	0.94	-0.50	0.019
<i>anti</i> -[8-OO-9MG] <sup>•+</sup>	-1.33	-1.28	-1.15	-0.28	-0.58	0.019
TS8b	-1.17	-1.13	-0.98	-0.08	-0.54	0.019
TS8c	-1.20	-0.23	-1.03	0.82	-0.84	0.020
<i>syn</i> -[8OO-9MG] <sup>•+</sup>	-1.40	-1.35	-1.23	-0.33	-0.78	0.019
TS8d	0.25	0.24	0.38	1.47	0.70	0.023
TS4a	-0.50	-0.45	-0.27	1.44	0.06	0.020
<i>anti</i> -[4OO-9MG] <sup>•+</sup>	-0.48	-0.46	-0.29	0.70	0.13	0.020
TS4b	-0.39	-0.40	-0.24	0.70	0.20	0.019
TS4c	-0.49	-0.47	-0.30	0.89	0.19	0.020
<i>syn</i> -[4-OO-9MG] <sup>•+</sup>	-0.49	-0.48	-0.35	0.61	0.12	0.020
TS 4d	0.07	0.09	0.29	1.38	0.61	0.022
TS5a	-1.02	-0.21	-0.84	0.03	-0.71	0.020
<i>anti</i> -[5-OO-9MG] <sup>•+</sup>	-1.16	-1.10	-0.96	0.02	-0.59	0.020
TSSb	-1.09	-1.04	-0.90	0.19	-0.53	0.019
TSSc	-1.07	-0.28	-0.89	0.95	0.88	0.020
<i>syn</i> -[5-OO-9MG] <sup>•+</sup>	-1.16	-1.11	-0.97	-0.04	-0.58	0.020
TS 5d	0.16	1.19	0.71	1.49	0.82	0.048
TS5e	-0.16	0.12	0.14	1.16	0.49	0.025
[4,5-OO-9MG] <sup>•+</sup>	-0.18	0.38	0.08	1.24	0.59	0.023

<sup>a</sup>Using  $\omega$ B97XD/6-31+G(d,p)-calculated geometries and thermal corrections. <sup>b</sup>CASSCF(9,7)/6-31+G(d,p) was used for 9MG<sup>•+</sup>, and CASSCF(12,8)/6-31+G(d,p) was used for <sup>1</sup>O<sub>2</sub>. <sup>c</sup>CASPT2(9,7)/6-31G(d,p) was used for 9MG<sup>•+</sup>, and CASPT2(12,8)/6-31G(d,p) was used for <sup>1</sup>O<sub>2</sub>.

facile and thermodynamically favorable. *syn*-[8-OO-9MG]<sup>•+</sup> may serve as an intermediate for a ring-closure reaction to [5,8-OO-9MG]<sup>•+</sup>, *i.e.*, the nucleophilic attack of the distal O atom of the peroxy group at the C5 atom *via* TS8d. In this sense, cycloaddition proceeds stepwise. The subsequent barrier TS8d for ring closure is significantly higher than the initial barrier TS8a (or TS8c) for <sup>1</sup>O<sub>2</sub> addition but is comparable to the barrier TSS8 for concerted cycloaddition. The unpaired electron is delocalized among the imidazole ring and O<sub>2</sub> in TS8a, TS8c, and TS8d and completely shifts to the  $\pi^*_{\text{O-O}}$  orbital in TS8b and *anti*- and *syn*-[8-OO-9MG]<sup>•+</sup>. As a result, the spin-charge separation increases continuously along the reaction pathways.

(3 and 4) C4- and C5-terminal addition of O<sub>2</sub> (shown by green and blue lines in Figure 2b, respectively). The two pathways follow a similar pattern. The C4-addition produces an *anti*-[4-OO-9MG]<sup>•+</sup> *via* TS4a and a *syn*-[4-OO-9MG]<sup>•+</sup> *via* TS4c. The two rotamers of [4-OO-9MG]<sup>•+</sup> may interconvert *via* TS4b, and *syn*-[4-OO-9MG]<sup>•+</sup> may convert to *syn*-[5-OO-9MG]<sup>•+</sup> *via* TS4d. Similarly, the C5-addition produces *anti*- and *syn*-[5-OO-9MG]<sup>•+</sup>. In both C4- and C5-peroxides, the barriers for rotation are small and the *syn*-conformers may be slightly more stable, analogous to the pair of *anti*- and *syn*-C8-peroxides. *syn*-[5-OO-9MG]<sup>•+</sup> may follow a stepwise cycloaddition to form [5,8-OO-9MG]<sup>•+</sup> *via* TS 5d or a dioxetane [4,5-OO-9MG]<sup>•+</sup> *via* TSSe. An interesting finding is that the formation of [4,5-OO-9MG]<sup>•+</sup> could be initiated only at [5-OO-9MG]<sup>•+</sup> but not at [4-OO-9MG]<sup>•+</sup>.

The spin-charge separation was also observed along the C4- and C5-addition pathways. While the positive charge is localized at the imidazole ring, the spin density is shared among the imidazole and the  $\pi^*_{\text{O-O}}$  orbital in TS4a (mostly on O<sub>2</sub>), TS4c (mostly on O<sub>2</sub>), TS4d (mostly on O<sub>2</sub>), TS5a, TSSc, TSSd, TS5e, and [4,5-OO-9MG]<sup>•+</sup>, and completely relocated to the  $\pi^*_{\text{O-O}}$  orbital in TS4b, TS5b, *anti*- and *syn*-[4-OO-9MG]<sup>•+</sup>, and *anti*- and *syn*-[5-OO-9MG]<sup>•+</sup>.

**3.2.2. Reaction Energies at the Single-Reference Levels and T1 Diagnostic.** Table 1 compares reaction enthalpies calculated at the  $\omega$ B97XD/6-31+G(d,p), RI-MP2/aug-cc-pVQZ, and DLPNO-CCSD(T)/aug-cc-pVTZ levels of theory. Reaction PESs constructed at the RI-MP2 and DLPNO-CCSD(T) levels are presented in the Supporting Information. On the one hand, the three different theories have predicted qualitatively similar reaction coordinates and pathways. Particularly, all peroxide-formation pathways are exothermic with no activation barriers above the reactants, except the TS8a calculated at RI-MP2. For each peroxide, the *anti*- and *syn*-conformers are comparable in terms of reaction activation barrier and product heat of formation, with the *syn*-conformer being slightly more favored. Of the three peroxides, [8-OO-9MG]<sup>•+</sup> has the lowest energy, followed by [5-OO-9MG]<sup>•+</sup> and then [4-OO-9MG]<sup>•+</sup>. On the other hand, the three theories have given rise to sizable differences in the reaction energies. For the formation of [5,8-OO-9MG]<sup>•+</sup>, the  $\omega$ B97XD and DLPNO-CCSD(T)-calculated barriers are 0.2–0.35 eV above the reactants, whereas the RI-MP2 barrier is 0.26 eV below the reactants. The formation of [4,5-OO-9MG]<sup>•+</sup> was



calculated to be exothermic at  $\omega$ B97XD but becomes endothermic at RI-MP2 and DLPNO-CCSD(T). Large deviations (from 0.79 eV up to 1.13 eV) were also observed in the reaction enthalpies of the precursor complex as well as TS8a, TS8c, TS5a, TS5c, and TS5d. As the reaction approaches the C8-, C5-, and C4- peroxides and 5,8-endoperoxide, the energies at the three levels are getting close and the differences decrease to  $\leq 0.24$  eV.

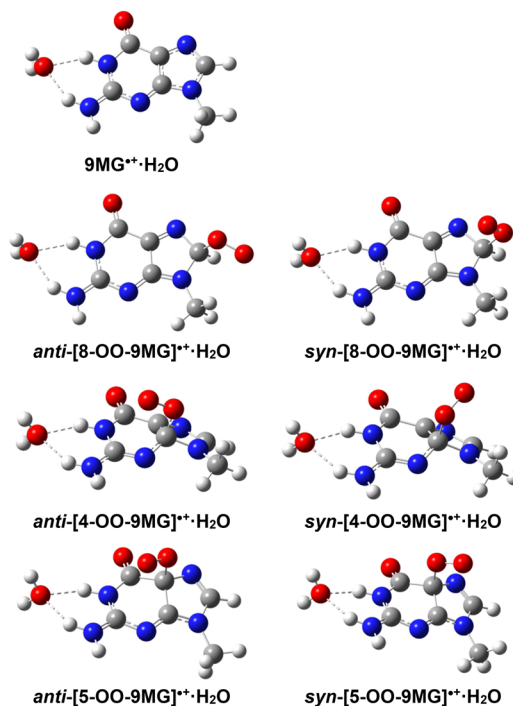
As aforementioned, single Slater-determinant wave functions may not be reliable in describing the open-shell electronic structures of  $^1\text{O}_2$  and its complexes with guanine radical cation. To quantitatively assess whether the calculated structures are dominated by single-determinant wave functions, a T1 diagnostic<sup>90,91</sup> was performed at the CCSD(T)/aug-cc-pVTZ level of theory for all of the structures. For a closed-shell system, a T1 diagnostic larger than 0.02 implies that the system is not well-described by a single-reference method. There exist other important configurations that are needed as references in a treatment of nondynamic electron correlation.<sup>90</sup> However, it is less clear what exactly constitutes a suspiciously large T1 for an open-shell system.<sup>91–93</sup> In the present work, the T1 diagnostic was used to mainly compare various species on the reaction PES and explore how the multireference character evolves along each reaction pathway.

The T1 diagnostic results of the coupled-cluster wave functions are collected in Table 1. Among the stationary structures, the precursor complex and [4,5-OO-9MG]<sup>•+</sup> have T1 exceeding 0.02. Besides, the TSs that lead to the formation of endoperoxides from peroxides (*i.e.*, TS5d leading from *syn*-[5-OO-9MG]<sup>•+</sup> to [5,8-OO-9MG]<sup>•+</sup>, TS5e from *syn*-[5-OO-9MG]<sup>•+</sup> to [4,5-OO-9MG]<sup>•+</sup>, and TS8d from *syn*-[8-OO-9MG]<sup>•+</sup> to [5,8-OO-9MG]<sup>•+</sup>), and the TS4d for the interconversion between *syn*-[4-OO-9MG]<sup>•+</sup> and *syn*-[5-OO-9MG]<sup>•+</sup> have T1 larger than 0.02. Coincidentally, these structures have the spin density delocalized among the imidazole ring and the O<sub>2</sub> orbital. This demonstrates a strong correlation between spin density distribution and T1 diagnostic.

**3.2.3. Experimental Benchmark for Reaction Thermodynamics.** Because the reaction product of 9MG<sup>•+</sup>·H<sub>2</sub>O corresponds to the O<sub>2</sub> addition accompanying elimination of a water ligand, the heat release from  $^1\text{O}_2$  oxidation must be larger than the water ligand elimination energy (or product ion hydration energy). Only in this case, the water molecule can be liberated barrierlessly following the O<sub>2</sub> addition.

Scheme 2 illustrates the structures of monohydrated 9MG<sup>•+</sup> and its peroxide products. Table 2 compares the water ligand elimination energies ( $\Delta H_{\text{water-eli}}$ ) of these peroxides at the single-reference levels. Assuming that spin contamination in the peroxides is similar in the absence and the presence of a water ligand, its effect tends to largely cancel out on water ligand elimination. As a result, the  $\omega$ B97XD, RI-MP2, and DLPNO-CCSD(T) methods have shown a good agreement (within 0.1 eV) in the  $\Delta H_{\text{water-eli}}$  value for each peroxide. On average, the water ligand elimination energy is 0.7 eV. On the basis of this experimental evidence, all of the reaction pathways which have an exothermicity over 0.7 eV and an activation barrier below the reactants could be detected in our experiment. The *anti*- and *syn*-conformers of [5-OO-9MG]<sup>•+</sup> and [8-OO-9MG]<sup>•+</sup> have exothermicity greater than 0.7 eV and therefore may be considered as probable products. On the other hand, *anti*- and *syn*-[4-OO-9MG]<sup>•+</sup>, [5,8-OO-9MG]<sup>•+</sup>, and [4,5-OO-9MG]<sup>•+</sup> either have a formation exothermicity

**Scheme 2. Lowest-Energy Structures of Monohydrated 9MG<sup>•+</sup> and Its Peroxide Products Optimized at the  $\omega$ B97XD/6-31+G(d,p) Level of Theory<sup>a</sup>**



<sup>a</sup>Their Cartesian coordinates are available in the Supporting Information.

**Table 2. Comparison of Water Ligand Elimination Energy ( $\Delta H_{\text{water-eli}}$ , eV) for Various Monohydrated Peroxide Products at the Single-Reference Levels of Theory**

species	$\omega$ B97XD/ 6-31+G(d,p)	RI-MP2/ aug-cc-pVQZ <sup>a</sup>	DLPNO- CCSD(T)/ aug-cc-pVTZ <sup>a</sup>
<i>anti</i> -[8-OO-9MG] <sup>•+</sup> ·H <sub>2</sub> O	0.79	0.71	0.69
<i>syn</i> -[8-OO-9MG] <sup>•+</sup> ·H <sub>2</sub> O	0.79	0.70	0.69
<i>anti</i> -[4-OO-9MG] <sup>•+</sup> ·H <sub>2</sub> O	0.73	0.64	0.63
<i>syn</i> -[4-OO-9MG] <sup>•+</sup> ·H <sub>2</sub> O	0.72	0.64	0.63
<i>anti</i> -[5-OO-9MG] <sup>•+</sup> ·H <sub>2</sub> O	0.79	0.71	0.70
<i>syn</i> -[5-OO-9MG] <sup>•+</sup> ·H <sub>2</sub> O	0.79	0.70	0.70

<sup>a</sup>Using  $\omega$ B97XD/6-31+G(d,p)-calculated geometries and thermal corrections.

much less than 0.7 eV or involve an activation barrier above the reactants and therefore may not be captured in the experiment. Of course, the calculations of reaction enthalpies have suffered spin contamination at the single-reference levels; as such, the analysis for experimental products needs to be validated at the multireference levels as discussed below.

**3.2.4. Reaction Energies at the Multireference Levels and Importance of Dynamic Electron Correlation.** Finally, reaction PESs were explored at the CASSCF(21,15)/6-31+G(d,p) and CASPT2(21,15)/6-31G(d,p) levels of theory. Their reaction energies are appended to Table 1, and their PESs are compared in Figure 3. The CASSCF and CASPT2-calculated reaction pathways have followed the same reaction coordinates as those predicted by the single-reference calculations. In addition, there is a good correlation between the spin density distributions determined at  $\omega$ B97XD and the SOMO orbitals mapped at CASSCF and CASPT2. However,



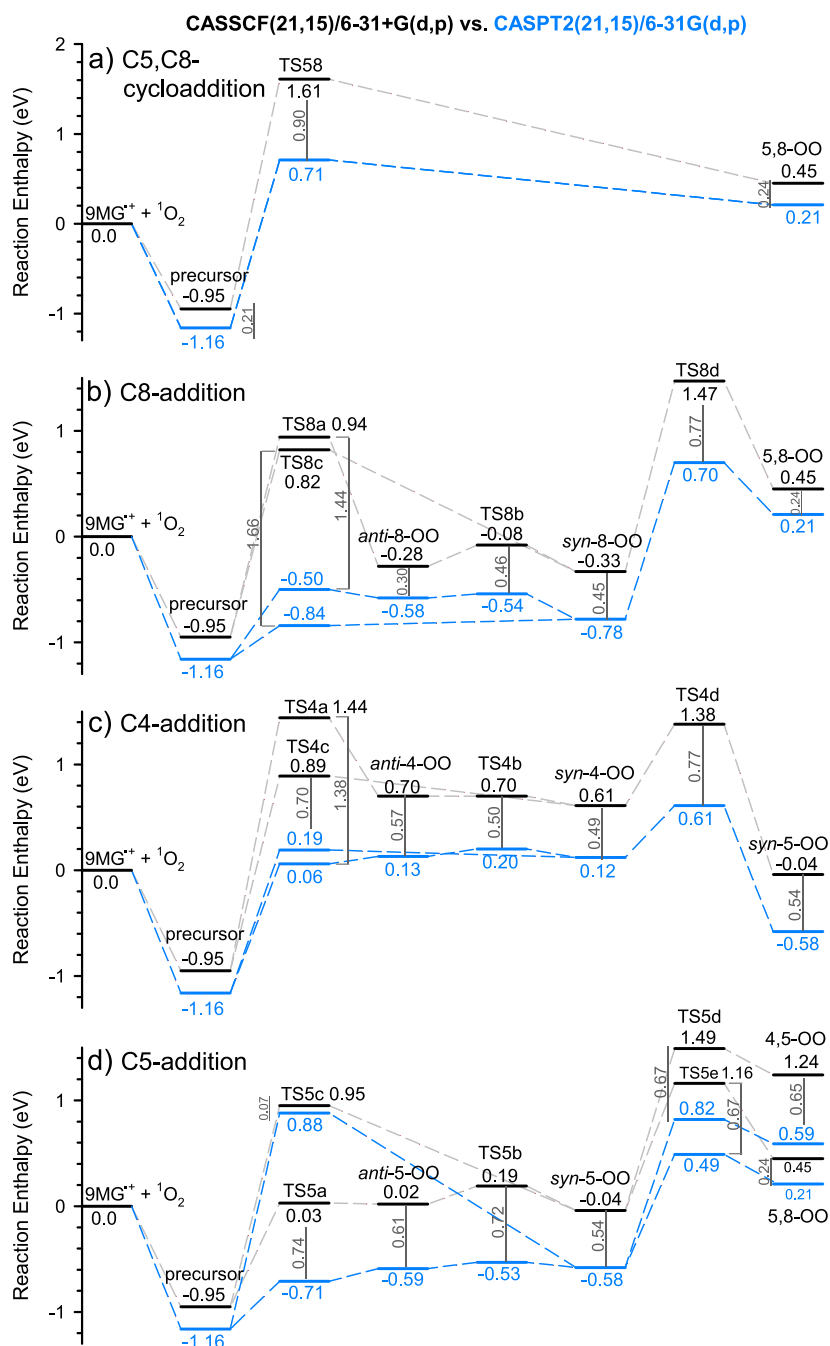


**Figure 3.** Comparison of multiconfiguration PES for the  $^1\text{O}_2$  addition to  $9\text{MG}^{*\text{+}}$  calculated at the CASSCF(21e,15o)/6-31+G(d,p) and CASPT2(21e,15o)/6-31G(d,p) levels of the theory, using the  $\omega\text{B97XD}/6-31+G(d,p)$ -optimized geometries. Reaction enthalpies were calculated at 298 K including thermal corrections.

the CASSCF calculations have significantly increased reaction energies. According to the CASSCF results, the *anti*- and *syn*-[8-OO-9MG] $^{*\text{+}}$  are the only two exothermic product channels (reaction  $\Delta H$  is  $-0.28$  and  $-0.33$  eV, respectively), but both bear a significant activation barrier (0.94 and 0.82 eV, respectively). These energies are clearly overestimated; otherwise, there would have been no products detected in our experiment. This indicates that CASSCF is problematic in treating the reaction of  $^1\text{O}_2$  with radicals. A similar problem was reported for the reaction of  $^1\text{O}_2$  with neutral guanine molecule by Schlegel and co-workers,<sup>43</sup> in which the addition barriers and the energies of the reaction intermediates were overestimated by CASSCF.

As rationalized above, a major problem of CASSCF is that it includes primarily nondynamic electron correlation. To improve the agreement with experiment, second-order perturbation theory corrections are required to account for dynamic correlation. For example, a composite CASPT2/DFT approach (*i.e.*, single-point CASPT2 energy calculations of open-shell geometries optimized at DFT) was found to produce correct PESs for the  $^1\text{O}_2$  reactions with alkenes<sup>72</sup> and 1,3-cyclohexadiene,<sup>43,94</sup> and the predicted barrier energies were consistent with the experimental data. A more related work was reported by Marchetti and Karsili,<sup>95</sup> in which CASPT2 was used to explore the  $^1\text{O}_2$  addition to neutral guanine and histidine. Inspired by these works, we have refined

the PES at CASPT2(21,15)/6-31G(d,p). As a calibration of the CASPT2 energy, we calculated the singlet–triplet energy gap of O<sub>2</sub> using CASPT2(12,8)/6-31G(d,p). CASPT2 predicted an excitation energy of 1.04 eV for <sup>1</sup>O<sub>2</sub>, close to the experimental value of 0.98 eV.<sup>62</sup> The superior performance of CASPT2 over CASSCF can be seen in detail in Figure 3, wherein the differences between the CASSCF and CASPT2 energies are indicated. It appears that dynamic correlations are the most significant in TS58 (0.90 eV), TS8a (1.44 eV), TS8c (1.66 eV), and TS4a (1.38 eV), where the numbers in the parentheses represent the energy corrections by CASPT2. The energy correction for dynamic correlation becomes less prominent as the reaction approaches the end products.

Note that, for most reaction species, the CASPT2 energy is 0.5–0.7 eV higher than the ωB97XD energy. This energy difference closely matches the amount of excitation energy that was overestimated (0.7 eV) for the <sup>1</sup>O<sub>2</sub> reactant by the spin-restricted ωB97XD. The exceptions are some *syn*-O<sub>2</sub> addition barriers, for which the CASPT2 and ωB97XD energies differ either less than 0.4 eV (*i.e.*, TS8c) or more than 1.9 eV (*i.e.*, TS5c). The RI-MP2 method also overstabilized reaction species in comparison to CASPT2 by a variable range from 0.2 to 1.2 eV, except TS8a, TS8c, TS5a, and TS 5d for which the energies increased at RI-MP2. Similarly, the DLPNO-CCSD(T) method overstabilized species by a range of 0.2–1.8 eV, except that the precursor complex became less stable by 0.52 eV with respect to CASPT2.

On the basis of the CASPT2 PES, the most probable experimental product channel corresponds to reactants → precursor → TS8c → *syn*-[8-OO-9MG]<sup>•+</sup> (the barrier TS8c has shifted to an energy below the product; thus, the reaction becomes barrierless), followed by reactants → precursor → TS8a → *anti*-[8-OO-9MG]<sup>•+</sup> → TS8b → *syn*-[8-OO-9MG]<sup>•+</sup>. Both *anti*- and *syn*-[8-OO-9MG]<sup>•+</sup> products have formation exothermicities above (or close to) 0.7 eV and no activation barriers above the reactants. The product exothermicity of *anti*- and *syn*-[5-OO-9MG]<sup>•+</sup> is only ~0.1 eV less than the water ligand elimination energy, so the formation of these product ions is possible at *E*<sub>col</sub> above 0.1 eV. The CASPT2 PES also suggests that 5,8-cycloaddition, 4,5-addition, and C4-terminal addition are endothermic and thus could be ruled out in the experiment.

**3.2.5. Comparison with the <sup>1</sup>O<sub>2</sub> Oxidation of [9MG + H]<sup>+</sup> and [9MG – H]<sup>–</sup>.** We have previously reported experimental and computational studies of the <sup>1</sup>O<sub>2</sub> reactions with [9MG + H]<sup>+</sup>·H<sub>2</sub>O (protonated at the N7 position) and [9MG – H]<sup>–</sup>·H<sub>2</sub>O (deprotonated at the N1 position).<sup>45</sup> The <sup>1</sup>O<sub>2</sub> oxidation of [9MG + H]<sup>+</sup> is dominated by a concerted 5,8-cycloaddition, and the [5,8-OO-9HG + H]<sup>+</sup> endoperoxide appeared as the only product. The same type of reaction becomes the least probable for 9MG<sup>•+</sup>. A concerted cycloaddition does not occur for [9MG – H]<sup>–</sup>. Instead, the <sup>1</sup>O<sub>2</sub> addition to [9MG – H]<sup>–</sup> is mediated by a stepwise addition starting with the formation of a [8-OO-9MG – H]<sup>–</sup> peroxide, which subsequently evolves to a [4,8-OO-9MG – H]<sup>–</sup> endoperoxide. Besides, no [5,8-OO-9MG – H]<sup>–</sup> endoperoxide could be formed in the reaction. The distinctively different oxidation pathways for 9MG<sup>•+</sup>, [9MG + H]<sup>+</sup>, and [9MG – H]<sup>–</sup> have reinforced the premise that different ionization states lead to different guanine oxidation mechanisms.

Similar to that of the guanine radical cation, the N9-methyl substitution in the protonated and deprotonated guanine ions decreases their reaction efficiencies with <sup>1</sup>O<sub>2</sub>, *i.e.*, the reaction

efficiency is 2.4% for [9HG + H]<sup>+</sup>·H<sub>2</sub>O and [9HG – H]<sup>–</sup>·H<sub>2</sub>O,<sup>44</sup> decreasing to 1.3–1.7% for [9MG + H]<sup>+</sup>·H<sub>2</sub>O and [9MG – H]<sup>–</sup>·H<sub>2</sub>O,<sup>45</sup> all of which were measured at 0.1 eV.

## 4. CONCLUSIONS

The present work is aimed at assessing the chemistry of the guanine radical cation with electronically excited <sup>1</sup>O<sub>2</sub> for the first time. The reactions for <sup>1</sup>O<sub>2</sub> with 9HG<sup>•+</sup>, 9MG<sup>•+</sup>, dGuo<sup>•+</sup>, and Guo<sup>•+</sup> were measured in the gas phase using guided-ion-beam scattering mass spectrometry. All of the reactions produced peroxide product ions, with the reaction cross sections in the order of 9HG<sup>•+</sup> > 9MG<sup>•+</sup> > dGuo<sup>•+</sup> ≈ Guo<sup>•+</sup>. These reactions were all found to be exothermic with no reaction barriers above the starting reactants, and the product exothermicities are above 0.7 eV. 9MG<sup>•+</sup> was chosen as a model compound to explore the reaction PES for the <sup>1</sup>O<sub>2</sub> oxidation of guanine radical cation computationally. The ωB97XD, RI-MP2, DLPNO-CCSD(T), CASSCF, and CASPT2 levels of theory have been each applied to the PES calculations. The different levels of theory have all predicted four reaction routes: a concerted 5,8-cycloaddition to the formation of an endoperoxide [5,8-OO-9MG]<sup>•+</sup> and C8-, C4-, and C5-terminal addition pathways to the formation of various peroxides ([8-OO-9MG]<sup>•+</sup>, [4-OO-9MG]<sup>•+</sup>, and [5-OO-9MG]<sup>•+</sup>) and then to a dioxetane [4,5-OO-9MG]<sup>•+</sup>. However, because of the multireference characters in the mixed open- and closed-shell <sup>1</sup>O<sub>2</sub> and in the open-shell <sup>1</sup>O<sub>2</sub>-adducts and transition states, the single-determinant reference calculations have suffered spin contamination, while the CASSCF struggled for a lack of a treatment of dynamic electron correlation. A successful approach was to use CASPT2 which couples complete active space with the corrections for dynamic correlation by second-order perturbation theory. The CASPT2-predicted reaction PES is consistent with the experimental measurement of reaction activation barrier and product enthalpy. Guided by experimental and computational evidence, it was predicted that the most probable reaction pathway for the oxidation of guanine radical cation corresponds to the formation of 8-peroxide. The formation of 5-peroxide may be possible in the experiment, but the formation of 4-peroxide, 5,8-endoperoxide, or 4,5-dioxetane were ruled out on the basis of unfavorable reaction barrier and/or reaction endothermicity. Finally, the distinctively different <sup>1</sup>O<sub>2</sub> reaction pathways of guanine radical cation compared to those of protonated and deprotonated guanine ions reported before have emphasized the dependence of the nucleobase oxidation mechanism on ionization states.

## ■ ASSOCIATED CONTENT

### Supporting Information

The Supporting Information is available free of charge at <https://pubs.acs.org/doi/10.1021/acs.jpca.1c00095>.

PESs at RI-MP2/aug-cc-pVQZ and DLPNO-CCSD(T)/aug-cc-pVTZ and Cartesian coordinates for the calculated structures (PDF)

## ■ AUTHOR INFORMATION

### Corresponding Author

Jianbo Liu – Department of Chemistry and Biochemistry, Queens College of the City University of New York, Queens, New York 11367, United States; Ph.D. Program in Chemistry, The Graduate Center of the City University of

New York, New York 10016, United States; [orcid.org/0000-0001-9577-3740](https://orcid.org/0000-0001-9577-3740); Phone: 1-718-997-3271; Email: [jianbo.liu@qc.cuny.edu](mailto:jianbo.liu@qc.cuny.edu)

## Authors

**Yan Sun** – Department of Chemistry and Biochemistry, Queens College of the City University of New York, Queens, New York 11367, United States; Ph.D. Program in Chemistry, The Graduate Center of the City University of New York, New York 10016, United States

**Midas Tsai** – Department of Natural Sciences, LaGuardia Community College, Long Island City, New York 11101, United States

**May Myat Moe** – Department of Chemistry and Biochemistry, Queens College of the City University of New York, Queens, New York 11367, United States; Ph.D. Program in Chemistry, The Graduate Center of the City University of New York, New York 10016, United States

Complete contact information is available at: <https://pubs.acs.org/10.1021/acs.jpca.1c00095>

## Notes

The authors declare no competing financial interest.

## ACKNOWLEDGMENTS

This work was supported by National Science Foundation (Grant No. CHE 1856362). Y.S. acknowledges CUNY Mina Rees Dissertation Fellowship. The authors are grateful to Prof. Jing Xie and Mr. Mengkai Liu (Beijing Institute of Technology) for guiding CASPT2 calculations. This work is dedicated to Prof. Cheuk-Yiu Ng. J.L. thanks Prof. Cheuk-Yiu Ng for inspiration and guidance in ion spectroscopy and dynamics.

## REFERENCES

- (1) Steenken, S.; Jovanovic, S. V. How Easily Oxidizable Is DNA? One-Electron Reduction Potentials of Adenosine and Guanosine Radicals in Aqueous Solution. *J. Am. Chem. Soc.* **1997**, *119*, 617–618.
- (2) Burrows, C. J.; Muller, J. G. Oxidative Nucleobase Modifications Leading to Strand Scission. *Chem. Rev.* **1998**, *98*, 1109–1151.
- (3) Zhou, J.; Kostko, O.; Nicolas, C.; Tang, X.; Belau, L.; de Vries, M. S.; Ahmed, M. Experimental Observation of Guanine Tautomers with VUV Photoionization. *J. Phys. Chem. A* **2009**, *113*, 4829–4832.
- (4) Schwell, M.; Hochlaf, M. Photoionization Spectroscopy of Nucleobases and Analogues in the Gas Phase Using Synchrotron Radiation as Excitation Light Source. *Top. Curr. Chem.* **2014**, *355*, 155–208.
- (5) Candeias, L. P.; Steenken, S. Structure and Acid-Base Properties of One-Electron-Oxidized Deoxyguanosine, Guanosine, and 1-Methylguanosine. *J. Am. Chem. Soc.* **1989**, *111*, 1094–9.
- (6) Steenken, S. Purine Bases, Nucleosides, and Nucleotides: Aqueous Solution Redox Chemistry and Transformation Reactions of Their Radical Cations and e<sup>-</sup> and OH Adducts. *Chem. Rev.* **1989**, *89*, 503–20.
- (7) Candeias, L. P.; Steenken, S. Ionization of Purine Nucleosides and Nucleotides and Their Components by 193-nm Laser Photolysis in Aqueous Solution: Model Studies for Oxidative Damage of DNA. *J. Am. Chem. Soc.* **1992**, *114*, 699–704.
- (8) Saito, I.; Nakamura, T.; Nakatani, K. Mapping of Highest Occupied Molecular Orbitals of Duplex DNA by Cobalt-Mediated Guanine Oxidation. *J. Am. Chem. Soc.* **2000**, *122*, 3001–3006.
- (9) Stemp, E. D. A.; Barton, J. K. Electron Transfer between Metal Complexes Bound to DNA: Is DNA a Wire? *Met. Ions Biol. Syst.* **1996**, *33*, 325–365.
- (10) Thorp, H. H. Cutting out the Middleman: DNA Biosensors Based on Electrochemical Oxidation. *Trends Biotechnol.* **1998**, *16*, 117–121.
- (11) Ribaut, C.; Bordeau, G.; Perio, P.; Reybier, K.; Sartor, V.; Reynes, O.; Fabre, P.-L.; Chouini-Lalanne, N. EPR Spectroelectrochemical Investigation of Guanine Radical Formation and Environment Effects. *J. Phys. Chem. B* **2014**, *118*, 2360–2365.
- (12) Kasai, H.; Yamaizumi, Z.; Berger, M.; Cadet, J. Photosensitized Formation of 7,8-Dihydro-8-oxo-2'-deoxyguanosine (8-Hydroxy-2'-deoxyguanosine) in DNA by Riboflavin: A Non Singlet Oxygen-Mediated Reaction. *J. Am. Chem. Soc.* **1992**, *114*, 9692–4.
- (13) Hall, J. P.; Poynton, F. E.; Keane, P. M.; Gurung, S. P.; Brazier, J. A.; Cardin, D. J.; Winter, G.; Gunnlaugsson, T.; Sazanovich, I. V.; Towrie, M.; et al. Monitoring One-Electron Photo-Oxidation of Guanine in DNA Crystals Using Ultrafast Infrared Spectroscopy. *Nat. Chem.* **2015**, *7*, 961–967.
- (14) Caruso, T.; Carotenuto, M.; Vasca, E.; Peluso, A. Direct Experimental Observation of the Effect of the Base Pairing on the Oxidation Potential of Guanine. *J. Am. Chem. Soc.* **2005**, *127*, 15040–15041.
- (15) Crespo-Hernández, C. E.; Close, D. M.; Gorb, L.; Leszczynski, J. Determination of Redox Potentials for the Watson-Crick Base Pairs, DNA Nucleosides, and Relevant Nucleoside Analogs. *J. Phys. Chem. B* **2007**, *111*, 5386–5395.
- (16) Hutter, M.; Clark, T. On the Enhanced Stability of the Guanine-Cytosine Base-Pair Radical Cation. *J. Am. Chem. Soc.* **1996**, *118*, 7574–7577.
- (17) Jaeger, H. M.; Schaefer, H. F. III, Characterizing Radiation-Induced Oxidation of DNA by Way of the Monohydrated Guanine-Cytosine Radical Cation. *J. Phys. Chem. B* **2009**, *113*, 8142–8148.
- (18) Lewis, F. D.; Liu, X.; Liu, J.; Miller, S. E.; Hayes, R. T.; Wasielewski, M. R. Direct Measurement of Hole Transport Dynamics in DNA. *Nature* **2000**, *406*, 51–53.
- (19) Cadet, J.; Berger, M.; Buchko, G. W.; Joshi, P. C.; Raoul, S.; Ravanat, J.-L. 2,2-Diamino-4-[(3,5-di-O-acetyl-2-deoxy-β-D-erythro-pentofuranosyl)amino]-5-(2H)-oxazolone: A Novel and Predominant Radical Oxidation Product of 3',5'-di-O-acetyl-2'-deoxyguanosine. *J. Am. Chem. Soc.* **1994**, *116*, 7403–4.
- (20) Cadet, J.; Douki, T.; Ravanat, J.-L. Oxidatively Generated Damage to the Guanine Moiety of DNA: Mechanistic Aspects and Formation in Cells. *Acc. Chem. Res.* **2008**, *41*, 1075–1083.
- (21) Neeley, W. L.; Essigmann, J. M. Mechanisms of Formation, Genotoxicity, and Mutation of Guanine Oxidation Products. *Chem. Res. Toxicol.* **2006**, *19*, 491–505.
- (22) Fleming, A. M.; Burrows, C. J. Formation and Processing of DNA Damage Substrates for the hNEIL Enzymes. *Free Radical Biol. Med.* **2017**, *107*, 35–52.
- (23) Boiteux, S.; Radicella, J. P. Base Excision Repair of 8-Hydroxyguanine Protects DNA from Endogenous Oxidative Stress. *Biochimie* **1999**, *81*, 59–67.
- (24) Ogilby, P. R. Singlet Oxygen: There Is Indeed Something New under the Sun. *Chem. Soc. Rev.* **2010**, *39*, 3181–3209.
- (25) *Singlet Oxygen: Applications in Biosciences and Nanosciences*, Vol. 1. In Compr. Ser. Photochem. Photobiol. Sci.; Nonell, S., Flors, C., Eds.; RSC: Cambridge, 2016.
- (26) Ravanat, J.-L.; Di Mascio, P.; Martinez, G. R.; Medeiros, M. H. G.; Cadet, J. Singlet Oxygen Induces Oxidation of Cellular DNA. *J. Biol. Chem.* **2000**, *275*, 40601–40604.
- (27) Cadet, J.; Douki, T.; Pouget, J.-P.; Ravanat, J.-L. Singlet Oxygen DNA Damage Products: Formation and Measurement. *Methods Enzymol.* **2000**, *319*, 143–153.
- (28) Cadet, J.; Ravanat, J.-L.; Martinez, G. R.; Medeiros, M. H. G.; Di Mascio, P. Singlet Oxygen Oxidation of Isolated and Cellular DNA: Product Formation and Mechanistic Insights. *Photochem. Photobiol.* **2006**, *82*, 1219–1225.
- (29) Cadet, J.; Douki, T.; Ravanat, J.-L. Oxidatively Generated Base Damage to Cellular DNA. *Free Radical Biol. Med.* **2010**, *49*, 9–21.
- (30) Sheu, C.; Foote, C. S. Endoperoxide Formation in a Guanosine Derivative. *J. Am. Chem. Soc.* **1993**, *115*, 10446–10447.



- (31) Ravanat, J.-L.; Douki, T.; Cadet, J. Direct and Indirect Effects of UV Radiation on DNA and Its Components. *J. Photochem. Photobiol. B* **2001**, *63*, 88–102.
- (32) Ravanat, J.-L.; Saint-Pierre, C.; Di Mascio, P.; Martinez, G. R.; Medeiros, M. H. G.; Cadet, J. Damage to Isolated DNA Mediated by Singlet Oxygen. *Helv. Chim. Acta* **2001**, *84*, 3702–3709.
- (33) Niles, J. C.; Wishnok, J. S.; Tannenbaum, S. R. Spiroiminodihydantoin Is the Major Product of the 8-Oxo-7,8-dihydroguanosine Reaction with Peroxynitrite in the Presence of Thiols and Guanosine Photooxidation by Methylene Blue. *Org. Lett.* **2001**, *3*, 963–966.
- (34) Kang, P.; Foote, C. S. Formation of Transient Intermediates in Low-Temperature Photosensitized Oxidation of an  $8\text{-}^{13}\text{C}$ -Guanosine Derivative. *J. Am. Chem. Soc.* **2002**, *124*, 4865–4873.
- (35) Ye, Y.; Muller, J. G.; Luo, W.; Mayne, C. L.; Shallop, A. J.; Jones, R. A.; Burrows, C. J. Formation of  $^{13}\text{C}$ -,  $^{15}\text{N}$ -, and  $^{18}\text{O}$ -Labeled Guanidinohydantoin from Guanosine Oxidation with Singlet Oxygen. Implications for Structure and Mechanism. *J. Am. Chem. Soc.* **2003**, *125*, 13926–13927.
- (36) Ravanat, J.-L.; Martinez, G. R.; Medeiros, M. H. G.; Di Mascio, P.; Cadet, J. Mechanistic Aspects of the Oxidation of DNA Constituents Mediated by Singlet Molecular Oxygen. *Arch. Biochem. Biophys.* **2004**, *423*, 23–30.
- (37) McCallum, J. E. B.; Kuniyoshi, C. Y.; Foote, C. S. Characterization of 5-Hydroxy-8-oxo-7,8-dihydroguanosine in the Photosensitized Oxidation of 8-Oxo-7,8-dihydroguanosine and Its Rearrangement to Spiroiminodihydantoin. *J. Am. Chem. Soc.* **2004**, *126*, 16777–16782.
- (38) Iesce, M. R.; Cermola, F.; Temussi, F. Photooxygenation of Heterocycles. *Curr. Org. Chem.* **2005**, *9*, 109–139.
- (39) Ravanat, J.-L.; Martinez, G. R.; Medeiros, M. H. G.; Di Mascio, P.; Cadet, J. Singlet Oxygen Oxidation of 2'-Deoxyguanosine. Formation and Mechanistic Insights. *Tetrahedron* **2006**, *62*, 10709–10715.
- (40) Gimisis, T.; Cismas, C. Isolation, Characterization, and Independent Synthesis of Guanine Oxidation Products. *Eur. J. Org. Chem.* **2006**, *2006*, 1351–1378.
- (41) Dumont, E.; Gruber, R.; Bignon, E.; Morell, C.; Moreau, Y.; Monari, A.; Ravanat, J.-L. Probing the Reactivity of Singlet Oxygen with Purines. *Nucleic Acids Res.* **2016**, *44*, 56–62.
- (42) Dumont, E.; Gruber, R.; Bignon, E.; Morell, C.; Aranda, J.; Ravanat, J.-L.; Tunon, I. Singlet Oxygen Attack on Guanine: Reactivity and Structural Signature within the B-DNA Helix. *Chem. - Eur. J.* **2016**, *22*, 12358–12362.
- (43) Thapa, B.; Munk, B. H.; Burrows, C. J.; Schlegel, H. B. Computational Study of Oxidation of Guanine by Singlet Oxygen ( $^1\Delta_g$ ) and Formation of Guanine:Lysine Cross-Links. *Chem. - Eur. J.* **2017**, *23*, 5804–5813.
- (44) Lu, W.; Liu, J. Capturing Transient Endoperoxide in the Singlet Oxygen Oxidation of Guanine. *Chem. - Eur. J.* **2016**, *22*, 3127–3138.
- (45) Lu, W.; Teng, H.; Liu, J. How Protonation and Deprotonation of 9-Methylguanine Alter Its Singlet  $\text{O}_2$  Addition Path: About the Initial Stage of Guanine Nucleoside Oxidation. *Phys. Chem. Chem. Phys.* **2016**, *18*, 15223–15234.
- (46) Lu, W.; Sun, Y.; Tsai, M.; Zhou, W.; Liu, J. Singlet  $\text{O}_2$  Oxidation of Deprotonated Guanine-Cytosine Base Pair and Its Entangling with Intra-Base-Pair Proton Transfer. *ChemPhysChem* **2018**, *19*, 2645–2654.
- (47) Lu, W.; Sun, Y.; Zhou, W.; Liu, J. Ph-Dependent Singlet  $\text{O}_2$  Oxidation Kinetics of Guanine and 9-Methylguanine: An Online Mass Spectrometry and Spectroscopy Study Combined with Theoretical Exploration. *J. Phys. Chem. B* **2018**, *122*, 40–53.
- (48) Sun, Y.; Tsai, M.; Zhou, W.; Lu, W.; Liu, J. Reaction Kinetics, Product Branching, and Potential Energy Surfaces of  $^1\text{O}_2$ -Induced 9-Methylguanine-Lysine Cross-Linking: A Combined Mass Spectrometry, Spectroscopy, and Computational Study. *J. Phys. Chem. B* **2019**, *123*, 10410–10423.
- (49) Bruner, S. D.; Norman, D. P. G.; Verdine, G. L. Structural Basis for Recognition and Repair of the Endogenous Mutagen 8-Oxoguanine in DNA. *Nature* **2000**, *403*, 859–866.
- (50) Marnett, L. J.; Burcham, P. C. Endogenous DNA Adducts: Potential and Paradox. *Chem. Res. Toxicol.* **1993**, *6*, 771–85.
- (51) Palumbo, G. Photodynamic Therapy and Cancer: A Brief Sightseeing Tour. *Expert Opin. Drug Delivery* **2007**, *4*, 131–148.
- (52) Munk, B. H.; Burrows, C. J.; Schlegel, H. B. An Exploration of Mechanisms for the Transformation of 8-Oxoguanine to Guanidinohydantoin and Spiroiminodihydantoin by Density Functional Theory. *J. Am. Chem. Soc.* **2008**, *130*, 5245–5256.
- (53) Ye, Y.; Munk, B. H.; Muller, J. G.; Cogbill, A.; Burrows, C. J.; Schlegel, H. B. Mechanistic Aspects of the Formation of Guanidinohydantoin from Spiroiminodihydantoin under Acidic Conditions. *Chem. Res. Toxicol.* **2009**, *22*, 526–535.
- (54) Colasanti, A.; Kisslinger, A.; Quarto, M.; Riccio, P. Combined Effects of Radiotherapy and Photodynamic Therapy on an *in Vitro* Human Prostate Model. *Acta Biochim. Polym.* **2004**, *51*, 1039–1046.
- (55) Postiglione, I.; Chiaviello, A.; Palumbo, G. Enhancing Photodynamic Therapy Efficacy by Combination Therapy: Dated, Current and Oncoming Strategies. *Cancers* **2011**, *3*, 2597–2629.
- (56) Lo, V. C. K.; Akens, M. K.; Moore, S.; Yee, A. J. M.; Wilson, B. C.; Whyne, C. M. Beyond Radiation Therapy: Photodynamic Therapy Maintains Structural Integrity of Irradiated Healthy and Metastatically Involved Vertebrae in a Pre-Clinical *in Vivo* Model. *Breast Cancer Res. Treat.* **2012**, *135*, 391–401.
- (57) Kobayashi, K.; Tagawa, S. Direct Observation of Guanine Radical Cation Deprotonation in Duplex DNA Using Pulse Radiolysis. *J. Am. Chem. Soc.* **2003**, *125*, 10213–10218.
- (58) Kobayashi, K.; Yamagami, R.; Tagawa, S. Effect of Base Sequence and Deprotonation of Guanine Cation Radical in DNA. *J. Phys. Chem. B* **2008**, *112*, 10752–10757.
- (59) Sun, Y.; Moe, M. M.; Liu, J. Mass Spectrometry and Computational Study of Collision-Induced Dissociation of 9-Methylguanine-1-Methylcytosine Base-Pair Radical Cation: Intra-Base-Pair Proton Transfer and Hydrogen Transfer, Non-Statistical Dissociation, and Reaction with a Water Ligand. *Phys. Chem. Chem. Phys.* **2020**, *22*, 14875–14888.
- (60) Midey, A.; Dotan, I.; Viggiano, A. A. Temperature Dependences for the Reactions of  $\text{O}^-$  and  $\text{O}_2^-$  with  $\text{O}_2(a^1\Delta_g)$  from 200 to 700 K. *J. Phys. Chem. A* **2008**, *112*, 3040–3045.
- (61) Fang, Y.; Liu, F.; Bennett, A.; Ara, S.; Liu, J. Experimental and Trajectory Study on Reaction of Protonated Methionine with Electronically Excited Singlet Molecular Oxygen ( $a^1\Delta_g$ ): Reaction Dynamics and Collision Energy Effects. *J. Phys. Chem. B* **2011**, *115*, 2671–2682.
- (62) Lafferty, W. J.; Solodov, A. M.; Lugez, C. L.; Fraser, G. T. Rotational Line Strengths and Self-Pressure-Broadening Coefficients for the 1.27  $\mu\text{m}$ ,  $a^1\Delta_g\text{-X}^3\Sigma_g^-$ ,  $= 0\text{-}0$  Band of  $\text{O}_2$ . *Appl. Opt.* **1998**, *37*, 2264–2270.
- (63) Liu, F.; Fang, Y.; Chen, Y.; Liu, J. Reactions of Deprotonated Tyrosine and Tryptophan with Electronically Excited Singlet Molecular Oxygen ( $a^1\Delta_g$ ): A Guided-Ion-Beam Scattering, Statistical Modeling, and Trajectory Study. *J. Phys. Chem. B* **2012**, *116*, 6369–6379.
- (64) Fang, Y.; Liu, J. Reaction of Protonated Tyrosine with Electronically Excited Singlet Molecular Oxygen ( $a^1\Delta_g$ ): An Experimental and Trajectory Study. *J. Phys. Chem. A* **2009**, *113*, 11250–11261.
- (65) Sun, Y.; Zhou, W.; Moe, M. M.; Liu, J. Reactions of Water with Radical Cations of Guanine, 9-Methylguanine, 2'-Deoxyguanosine and Guanosine: Keto-Enol Isomerization, C8-Hydroxylation, and Effects of N9-Substitution. *Phys. Chem. Chem. Phys.* **2018**, *20*, 27510–27522.
- (66) Cheng, P.; Bohme, D. K. Gas-Phase Formation of Radical Cations of Monomers and Dimers of Guanosine by Collision-Induced Dissociation of  $\text{Cu(II)}$ -Guanosine Complexes. *J. Phys. Chem. B* **2007**, *111*, 11075–11082.

- (67) Feketeová, L.; Yuriev, E.; Orbell, J. D.; Khairallah, G. N.; O'Hair, R. A. J. Gas-Phase Formation and Reactions of Radical Cations of Guanosine, Deoxyguanosine and Their Homodimers and Heterodimers. *Int. J. Mass Spectrom.* **2011**, *304*, 74–82.
- (68) Al-Sheikhly, M. The Reactivity of Adenyl and Guanyl Radicals Towards Oxygen. *Radiat. Phys. Chem.* **1994**, *44*, 297–301.
- (69) Chai, J.-D.; Head-Gordon, M. Long-Range Corrected Hybrid Density Functionals with Damped Atom-Atom Dispersion Corrections. *Phys. Chem. Chem. Phys.* **2008**, *10*, 6615–6620.
- (70) Kumar, A.; Sevilla, M. D. Proton Transfer Induced Somo-to-Homo Level Switching in One-Electron Oxidized A-T and G-C Base Pairs: A Density Functional Theory Study. *J. Phys. Chem. B* **2014**, *118*, 5453–5458.
- (71) Reynisson, J.; Steenken, S. DFT Calculations on the Electrophilic Reaction with Water of the Guanine and Adenine Radical Cations. A Model for the Situation in DNA. *Phys. Chem. Chem. Phys.* **2002**, *4*, 527–532.
- (72) Maranzana, A.; Ghigo, G.; Tonachini, G. Diradical and Peroxirane Pathways in the  $[\pi 2 + \pi 2]$  Cycloaddition Reactions of  $^1\Delta_g$  Dioxygen with Ethene, Methyl Vinyl Ether, and Butadiene: A Density Functional and Multireference Perturbation Theory Study. *J. Am. Chem. Soc.* **2000**, *122*, 1414–1423.
- (73) Saito, T.; Nishihara, S.; Kataoka, Y.; Nakanishi, Y.; Matsui, T.; Kitagawa, Y.; Kawakami, T.; Okumura, M.; Yamaguchi, K. Transition State Optimization Based on Approximate Spin-Projection (AP) Method. *Chem. Phys. Lett.* **2009**, *483*, 168–171.
- (74) Saito, T.; Nishihara, S.; Kataoka, Y.; Nakanishi, Y.; Kitagawa, Y.; Kawakami, T.; Yamanaka, S.; Okumura, M.; Yamaguchi, K. Reinvestigation of the Reaction of Ethylene and Singlet Oxygen by the Approximate Spin Projection Method. Comparison with Multireference Coupled-Cluster Calculations. *J. Phys. Chem. A* **2010**, *114*, 7967–7974.
- (75) Weigend, F.; Haser, M.; Patzelt, H.; Ahlrichs, R. RI-MP2: Optimized Auxiliary Basis Sets and Demonstration of Efficiency. *Chem. Phys. Lett.* **1998**, *294*, 143–152.
- (76) Jurecka, P.; Nachtigall, P.; Hobza, P. RI-MP2 Calculations with Extended Basis Sets 22a Promising Tool for Study of H-Bonded and Stacked DNA Base Pairs. *Phys. Chem. Chem. Phys.* **2001**, *3*, 4578–4582.
- (77) Liakos, D. G.; Sparta, M.; Kesharwani, M. K.; Martin, J. M. L.; Neese, F. Exploring the Accuracy Limits of Local Pair Natural Orbital Coupled-Cluster Theory. *J. Chem. Theory Comput.* **2015**, *11*, 1525–1539.
- (78) Roos, B. O.; Taylor, P. R.; Sigbahn, P. E. M. A Complete Active Space SCF Method (CAS-SCF) Using a Density Matrix Formulated Super-CI Approach. *Chem. Phys.* **1980**, *48*, 157–73.
- (79) Olsen, J.; Roos, B. O.; Jørgensen, P.; Jensen, H. J. A. Determinant Based Configuration Interaction Algorithms for Complete and Restricted Configuration Interaction Spaces. *J. Chem. Phys.* **1988**, *89*, 2185–2192.
- (80) Alecu, I. M.; Zheng, J.; Zhao, Y.; Truhlar, D. G. Computational Thermochemistry: Scale Factor Databases and Scale Factors for Vibrational Frequencies Obtained from Electronic Model Chemistries. *J. Chem. Theory Comput.* **2010**, *6*, 2872–2887.
- (81) Andersson, K.; Malmqvist, P. A.; Roos, B. O. Second-Order Perturbation Theory with a Complete Active Space Self-Consistent Field Reference Function. *J. Chem. Phys.* **1992**, *96*, 1218–26.
- (82) Abe, M.; Gopakmar, G.; Nakajima, T.; Hirao, K. Relativistic Multireference Perturbation Theory: Complete Active-Space Second-Order Perturbation Theory (CASPT2) with the Four-Component Dirac Hamiltonian. In *Radiation Induced Molecular Phenomena in Nucleic Acids*; Shukla, K., K., M., Leszczynski, J., Eds.; Springer: Netherlands, 2008; pp 157–177.
- (83) Buenker, R. J.; Peyerimhoff, S. D. Individualized Configuration Selection in CI Calculations with Subsequent Energy Extrapolation. *Theor. Chim. Acta* **1974**, *35*, 33–58.
- (84) Frisch, M. J.; Trucks, G. W.; Schlegel, H. B.; Scuseria, G. E.; Robb, M. A.; Cheeseman, J. R.; Scalmani, G.; Barone, V.; Mennucci, B.; Petersson, G. A.; et al. *Gaussian 09*, rev. D.01; Gaussian, Inc: Wallingford, CT, 2013.
- (85) Neese, F. Software Update: The Orca Program System, Version 4.0. *WIREs Comput. Mol. Sci.* **2018**, *8*, No. e1327.
- (86) Aquilante, F.; Autschbach, J.; Carlson, R. K.; Chibotaru, L. F.; Delcey, M. G.; De Vico, L.; Fdez Galvan, I.; Ferre, N.; Frutos, L. M.; Gagliardi, L.; et al. Molcas 8: New Capabilities for Multiconfigurational Quantum Chemical Calculations across the Periodic Table. *J. Comput. Chem.* **2016**, *37*, 506–541.
- (87) Roca-Sanjuán, D.; Rubio, M.; Merchán, M.; Serrano-Andrés, L. Ab Initio Determination of the Ionization Potentials of DNA and RNA Nucleobases. *J. Chem. Phys.* **2006**, *125*, 084302.
- (88) Ghigo, G.; Roos, B. O.; Malmqvist, P.-A. A Modified Definition of the Zeroth-Order Hamiltonian in Multiconfigurational Perturbation Theory (CASPT2). *Chem. Phys. Lett.* **2004**, *396*, 142–149.
- (89) Troe, J. Statistical Adiabatic Channel Model of Ion-Neutral Dipole Capture Rate Constants. *Chem. Phys. Lett.* **1985**, *122*, 425–430.
- (90) Lee, T. J.; Taylor, P. R. A Diagnostic for Determining the Quality of Single-Reference Electron Correlation Methods. *Int. J. Quantum Chem.* **1989**, *36*, 199–207.
- (91) Jayatilaka, D.; Lee, T. J. Open-Shell, Coupled-Cluster Theory. *J. Chem. Phys.* **1993**, *98*, 9734–47.
- (92) Rienstra-Kiracofe, J. C.; Allen, W. D.; Schaefer, H. F. The  $C_2H_5 + O_2$  Reaction Mechanism: High-Level Ab Initio Characterizations. *J. Phys. Chem. A* **2000**, *104*, 9823–9840.
- (93) Lee, T. J. Comparison of the T1 and D1 Diagnostics for Electronic Structure Theory: A New Definition for the Open-Shell D1 Diagnostic. *Chem. Phys. Lett.* **2003**, *372*, 362–367.
- (94) Sevin, F.; McKee, M. L. Reactions of 1,3-Cyclohexadiene with Singlet Oxygen. A Theoretical Study. *J. Am. Chem. Soc.* **2001**, *123*, 4591–4600.
- (95) Marchetti, B.; Karsili, T. N. V. An Exploration of the Reactivity of Singlet Oxygen with Biomolecular Constituents. *Chem. Commun.* **2016**, *52*, 10996–10999.